Suspended-Sediment Distribution Patterns in Tide-Dominated Estuaries on the Eastern Amazon Coast: Geomorphic Controls of Turbidity-Maxima Formation

Vando J. C. Gomes [1], Nils E. Asp [2,*], Eduardo Siegle [3], José Diego Gomes [1], Ariane M. M. Silva [4], Andrea S. Ogston [5] and Charles A. Nittrouer [5]

[1] Graduate Program on Environmental Biology (PPBA), Federal University of Pará (UFPA), Alam. Leandro Ribeiro, s/n—Campus UFPA, Bragança CEP: 68600-000, PA, Brazil; vandojcg@yahoo.com.br (V.J.C.G.); jdiegogv@hotmail.com (J.D.G.)

[2] Institute for Coastal Studies, Federal University of Pará (UFPA), Alam. Leandro Ribeiro, s/n—Bairro Aldeia Campus UFPA, Bragança CEP: 68600-000, PA, Brazil

[3] Oceanographic Institute, University of São Paulo (USP), São Paulo CEP: 05508-120, SP, Brazil; esiegle@usp.br

[4] Graduate Program on Geology and Geochemistry (PPGG), Federal University of Pará (UFPA), Rua Augusto Corrêa, 01—UFPA-Guamá, Belém CEP: 66075-110, PA, Brazil; ariianemarques@hotmail.com

[5] School of Oceanography, University of Washington (UW), Box 357940, Seattle, WA 98195-7940, USA; ogston@uw.edu (A.S.O.); nittroue@uw.edu (C.A.N.)

* Correspondence: nilsasp@ufpa.br

Abstract: In tide-dominated estuaries, maximum-turbidity zones (MTZs) are common and prominent features, characterized by a peak in suspended-sediment concentration (SSC) associated with estuarine processes. The Brazilian Amazon coast includes many estuaries, experiencing macrotidal conditions. MTZs are expected to occur and are crucial for sediment delivery to the longest continuous mangrove belt of the world. The area is under influence of the Amazon River plume (ARP), the main SSC source, as local rivers do not deliver substantial sediment supply. To assess the processes that allow the ARP to supply sediment to the estuaries and mangrove belt along the Amazon coast, the results from previous individual studies within five Amazon estuaries (Mocajuba, Taperaçu, Caeté, Urumajó and Gurupi) were compared with regards to SSC, salinity, morphology and tidal propagation. This comparison reinforces that these estuaries are subject to similar regional climate and tidal variations, but that their dynamics differ in terms of distance from the Amazon River mouth, importance of the local river sediment source, and morphology of the estuarine setting. The Urumajó, Caeté and Gurupi are hypersynchronous estuaries where perennial, classic MTZs are observed with SSC > 1 g·L^{-1}. This type of estuary results in transport convergence and MTZ formation, which are suggested to be the main processes promoting mud accumulation in the Amazonian estuaries and therefore the main means of mud entrapment in the mangrove belt. The Mocajuba and the Taperaçu estuaries showed synchronous and hyposynchronous processes, respectively, and do not present classic MTZs. In these cases, the proximity to the ARP for the Mocajuba and highly connected tidal channels for the Taperaçu estuary, assure substantial mud supply into these estuaries. This study shows the strong dependence of the estuaries and mangrove belt on sediment supply from the ARP, helping to understand the fate of Amazon River sediments and providing insights into the mechanisms providing sediment to estuaries and mangroves around the world, especially under the influence of big rivers.

Keywords: estuaries; suspended-sediment concentration; tidal prism; tides; turbidity

1. Introduction

Estuaries have been defined and classified based on different factors that reflect the diversity of coastal areas and scientific interests [1]. These different perspectives include

geomorphology and stratigraphy [2–4], the salinity gradient [5–7], biological aspects [8] and the circulation pattern and water stratification [9–11].

The basic consensus of these different perspectives is that estuaries are coastal, transitional between continental and marine environments where the continental and marine influences are manifested mainly in terms of salinity and tides. While variations in salinity stratification produce baroclinic conditions/circulation, tidal variations produce barotropic conditions/circulation. The baroclinic circulation has little relevance where the tidal variations are intense and the turbulence generates strong mixing of the estuarine waters, and the estuaries can thus be classified as vertically homogeneous, well mixed, or tide-dominated [11], in contrast to wave-dominated estuaries [3] or river-dominated estuaries [12]. These patterns are substantially influenced by friction, which in this context is mostly a product of the estuarine morphology (e.g., depth) [13,14]. Shallow depths in relation to the tidal range favor turbulence and mixing [15].

In estuaries where the tide is the main forcing, it dominates the transport processes, thus determining the estuarine geomorphological configuration, which is the case for the Brazilian Amazon coast. Estuaries receive sediments, especially in suspension from river/continental sources and from marine sources. Flocculation and salt wedges play a fundamental role in the sediment transport and accumulation in well stratified and/or wave-dominated estuaries, but the transport and accumulation are governed by the convergence of processes in tide-dominated and vertically homogeneous estuaries [16]. In both conditions, one feature of suspended-sediment transport is the formation of turbidity maxima or maximum-turbidity zones (MTZs), which are characterized by great values of suspended-sediment concentration (SSC) in a given sector of the estuary, located at or near to the head of the salt intrusion [11,17]. A turbidity maximum can develop in different ways [16,18]. Classical studies refer to density circulation [16] and tidal transport [18] as the general driving processes for MTZ formation in well-stratified and well-mixed estuaries, respectively. In all models, a longitudinal seaward dilution of river-borne SSC is considered, whereas a peak in SSC is reached near the landward limit of the salt intrusion [18].

In the case of tide-dominated estuaries, MTZs are relatively common phenomena (e.g., Ref. [19]). There is no particular SSC value that defines an MTZ, especially due to large differences in sediment availability [17]. Tidal conditions obviously affect the MTZ characteristics. In mesotidal estuaries, MTZs usually have SSC in the order of 0.1 to 0.2 $g·L^{-1}$, whereas hypertidal (i.e., tidal range > 6 m) estuaries present SSC of 1 to 10 $g·L^{-1}$ [11]. Herewith, we consider mean concentrations of > 0.5 $g·L^{-1}$ to characterize an MTZ, which is reasonable for macrotidal (tidal range 4–6 m) estuaries such as those along the Amazonian coast, and which is supported by previous studies [20].

In addition, the longitudinal convergence of transport and the MTZ are constantly experiencing spatial and temporal displacements as a function of the tidal cycle, the variation in tidal height as a function of the spring-neap cycle and seasonal variations as a function of the rainfall regime and river discharge [21–23]. Vertical circulation, tidal pumping and resuspension are the dominant mechanisms for the formation of the MTZ [17]. The location and turbidity of the MTZ in the estuaries are sensitive to variations in tidal phases and river-flow rates. Thus, comparative studies of estuaries from the same region subjected to the same geological and climate configuration, as well as similar tidal ranges, are particularly interesting if we aim to understand the dynamics of suspended sediments in estuaries and the formation of MTZs [18,24]. These processes are very important since they influence the morphodynamic evolution of estuaries, accumulation of contaminants, species migration, primary production, siltation, et cetera [25–27].

Several studies have sought to understand the mechanisms of formation and dynamics of the MTZ, such as in the Changjiang estuary [22,28] in China and Yalu estuary [29] in China/North Korea; the Gironde estuary in France [30]; the Humber and Ouse estuaries in the United Kingdom [31]; the Northern European estuaries of Weser, Seine, Scheldt and Humber [32]; and the Urumajó and Caeté estuaries [20,33] in the eastern sector of the Amazon coast. Even though Brazil has many estuarine systems, there are few studies about

the formation and dynamics of their MTZs. Additionally, there is a contrast between the occurrence of tide-dominated estuaries on the Amazon coast of Brazil and the rest of the estuaries along the Brazilian coast, where stratification and waves are more relevant [1].

The objective of this study is to investigate the variation in SSC and the factors controlling the formation of the MTZ in five different Amazon estuaries: Mocajuba, Taperaçu, Caeté, Urumajó and Gurupi. These estuaries are subject to similar regional climate and tidal variations, but there is a variation in distance from the Amazon River and its plume, a gradation of relative importance of the local river discharge and important morphological differences. In contrast to most estuaries where the local fluvial waters are the main source of suspended sediments here we investigate estuarine systems where the main SSC source lies offshore, to understand its impact on the MTZ formation.

Additionally, we tested the concept that despite variations in local fluvial discharge and geomorphic characteristics, all of these estuaries along the northeast Amazon coast would exhibit an MTZ. Seasonal variations are also evaluated, not only because of impacts from the local river components but also impacts from the Amazon River plume (ARP), which influences the regional conditions in many ways.

2. Study Area

The eastern sector of the Amazon coast covers the states of Pará and Maranhão (Figure 1b). It has >20 estuaries, which fit the definition of a tide-dominated estuary [3]. These estuaries are associated with an extensive mangrove belt of approximately 7600 km^2, which corresponds to approximately 75% of Brazilian mangroves [34,35]. It has been shown that this large mangrove occurrence is related to the Amazon River suspended-sediment supply [20,35], which decreases southeastwards.

Even though they have apparent physiographic similarity and the climate conditions have some regularity along the coast, the estuaries of the eastern sector of the Amazon coast have some distinct characteristics (geology, drainage-basin size, and river discharge), causing them to experience different hydrodynamic behavior [36]. In this context, the mechanisms for retention and transport of fine sediment in the eastern sector of the Amazon Coastal Zone (ACZ) are relevant because they are associated with the establishment and growth of extensive mangrove regions, where the amount of local river input of sediments is small [20,33,35]. In turn, the Amazon River represents the largest supply of continental water and discharge of suspended sediments to the oceans, as it annually delivers 6×10^{12} m^3 of water (17% of the world total) and 1.2×10^9 tons of sediment [37,38]. Although its plume is transported mainly to the northwest, seasonal drift to the southeast has been documented [38,39] and represents an important contribution of suspended sediments to the estuaries studied here (e.g., Ref. [20]), i.e., Mocajuba, Taperaçu, Caeté, Urumajó and Gurupi; Table 1).

Table 1. Key features of the investigated estuaries along the east sector of the Amazon coast.

Estuary	Distance from Amazon River Mouth (km)	Estuarine Length (km)	Catchment Area (km^2)	Mangrove Area (km^2)	River Discharge (m$^3 \cdot$s^{-1})
Mocajuba	225	53.0	323	54.5	11.0
Taperaçu	353	27.5	40	100.6	–
Caeté	369	54.3	2236	110.1	41.5
Urumajó	374	43.0	544	36.4	10.0
Gurupi	433	57.7	35,053	85.9	472.0

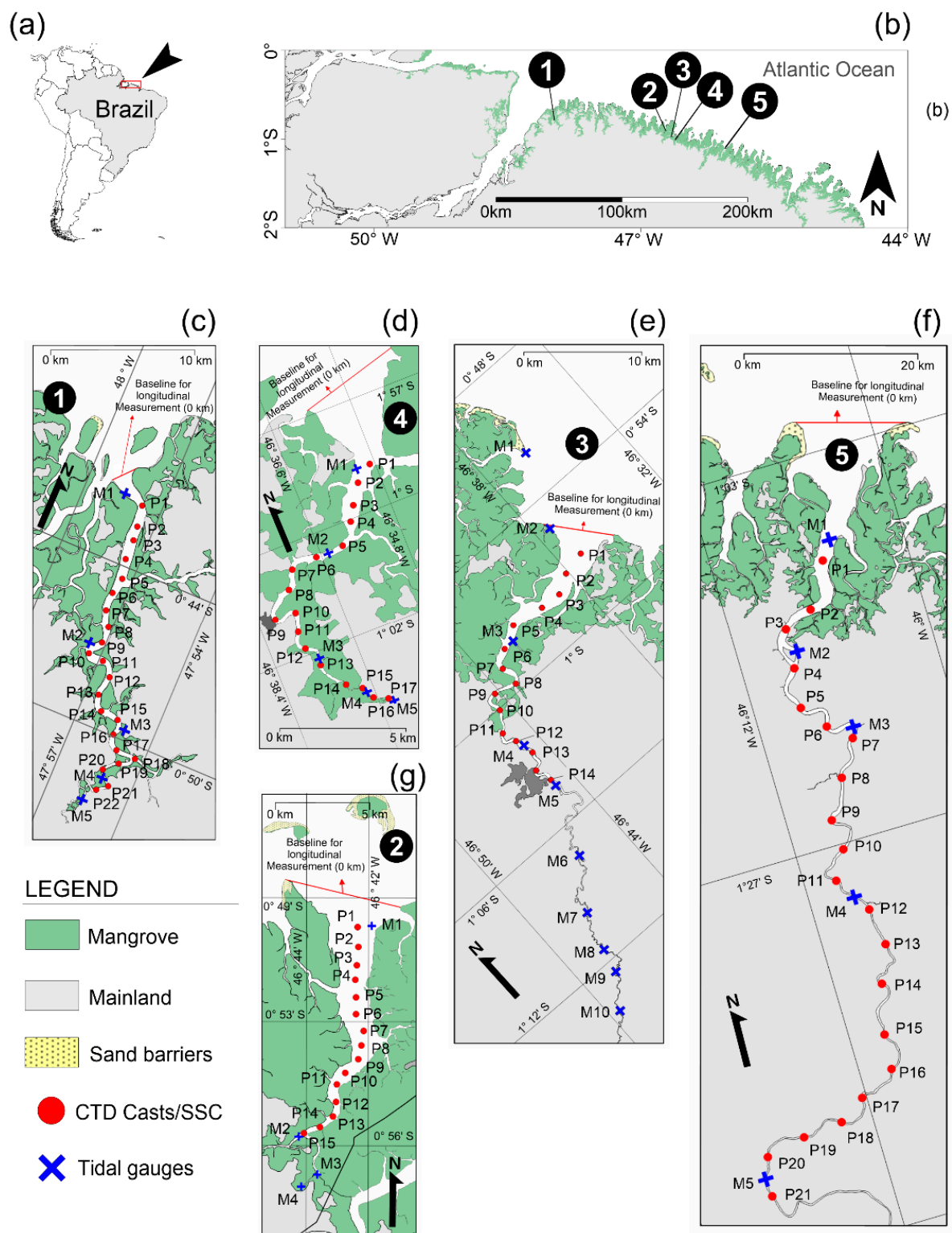**Figure 1.** Location of study sites (**a**), corresponding to the eastern sector of the Amazon coast (**b**), and the Mocajuba (**c**), Urumajó (**d**), Caeté (**e**), Gurupi (**f**) and Taperaçu (**g**) estuaries.

The Caeté River has a drainage basin of 2236 km^2 with a length of 110 km along the main river channel [36,40]. The record from the Nova Mocajuba hydrological station (Figure 1e) reveals a mean river discharge of 41.5 m$^3 \cdot$s^{-1}. For the month of November (dry season), the discharge is 7.03 m$^3 \cdot$s^{-1}; and for the month of April (rainy season), the discharge is 82.3 m$^3 \cdot$s^{-1} [41].

The Taperaçu estuary is classified as a frictionally dominated estuary with a mean depth of 4 m [42]. Its drainage basin is ~40 km^2 (Figure 1g), and the absence of an effective river discharge is among its peculiarities [42]. There is a hydrodynamic connection between the Caeté and Taperaçu estuaries through the tidal channels Furo Grande and Furo do Taici, which is a very important factor from the hydrodynamic [43–45] and biological points of view [46].

The estuary of the Urumajó River (Figure 1d) extends for ~50 km, and the area of its drainage basin is ~544 km^2, with a mean elevation of 34 m. The length of its estuarine region is ~20 km, and its mouth flows into Caeté Bay [33,42].

The Mocajuba River estuary (Figure 1c) has a river discharge ~27% of the Caeté River discharge [36]. Although there are no historical records, the maximum monthly mean river discharge and annual mean river discharge are estimated at 68.5 and 11 m^3·s^{-1}, respectively [47]. The area of its drainage basin is ~323 km^2 [47].

The estuary of the Gurupi River (Figure 1f) has a drainage basin of ~35,000 km^2 [35] and a mean flow rate of 472 m^3·s^{-1} [40]. The flow rate of the Gurupi River is estimated to be ~7 times greater in the rainy season (e.g., April–May ~1125 m^3·s^{-1}) than in the dry season (e.g., October–November ~155 m^3·s^{-1}). Similar to the other estuaries in this sector, the Gurupi River estuary has extensive mangroves occupying the coastal plains in its distal portion. In addition, there are several rocky outcrops in the area associated with the São Luís Craton [48].

The climate of the region is tropical, hot and humid, and is characterized by the occurrence of a rainy season from January to June and a dry season from August to November (Figure 2), with mean annual rainfall ranging between 2300 and 2800 mm [49]. The intertropical convergence zone (ITCZ) is one of the main factors responsible for the occurrence of rainfall in the region [50,51]. The ITCZ controls the seasonal rainfall patterns (Figure 2a), and modulates Amazon River discharge and its plume displacement due to seasonal wind pattern variation (Figure 2b) [38,49]. This seasonal pattern is particularly important because the area is not affected by tropical storms [52].
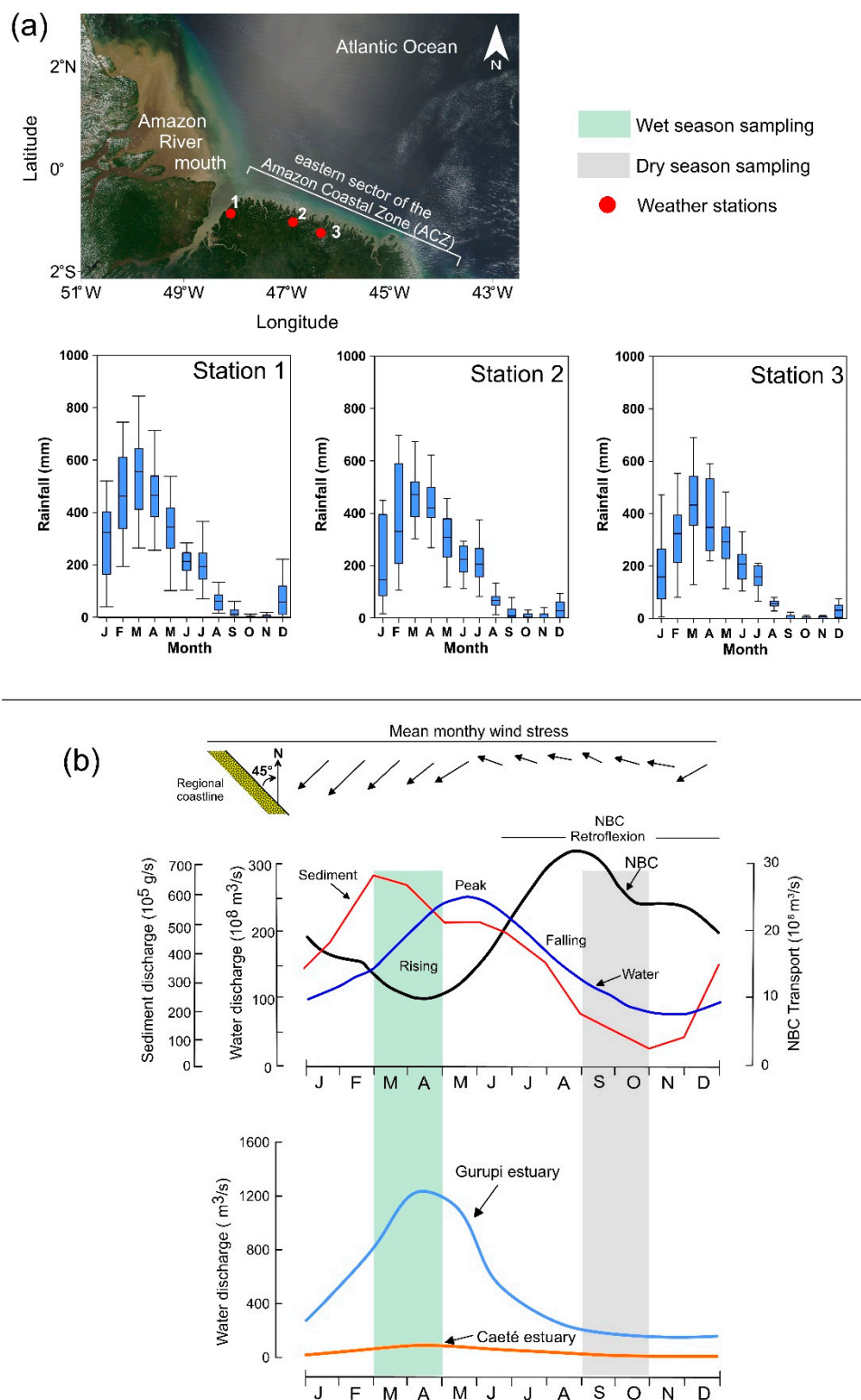
Figure 2. Climate conditions along the eastern portion of the Amazon coast. (**a**) Data from stations near the study areas, for 2000–2018, in the rain-gauge station for the municipality of Curuçá near the Mocajuba River estuary (left), the rain-gauge station for the municipality of Tracuateua, near the Taperaçu, Caeté, and Urumajó estuaries (middle), and the Viseu rain-gauge station near the Gurupi River estuary (right). (**b**) Scheme proposed by [42] for the dynamics of the Amazon River plume and discharge of the Gurupi River (Alto Bonito river station) and the Caeté River (Nova Mocajuba river station) for 2000–2014. The vertical bars show the data collection periods in the five estuaries: rainy season (green bar) and dry season (gray bar).

3. Materials and Methods

To evaluate the dynamics of suspended sediments in the five estuarine systems, the longitudinal and vertical changes in SSC under different tide and river-discharge conditions were investigated, along with salinity measurements. The Caeté River estuary is a representative of the tide-dominated estuary model, with medium and balanced conditions in terms of river morphology and flow rate [20,35,40]. Thus, a comparative approach was adopted based on knowledge of the Caeté River estuary and the assumption that this would be a representative condition for the other estuaries. In parallel, surveys of water-level changes were performed at various points in each estuary, along with morphology mapping of each system. These methods are detailed below.

3.1. Measurements of SSC and Salinity throughout the Estuaries

The SSC and salinity measurements were obtained from longitudinal surveys composed of regularly spaced vertical CTD profiles. These longitudinal surveys follow approximately the thalweg of the estuarine channels, close to the time of high-water. Due to differences of the boat path and to morphodynamic changes, the bottom track might differ seasonally in each estuary. In all five cases, surveys were performed during periods of high and low river discharge, generally during no-overbank tides (e.g., neap tides). Additional surveys were also conducted under overbank (spring) tide conditions, when the mangrove areas were flooded. Salinity and turbidity data were obtained through vertical profiles of conductivity, temperature, and depth CTD 90M probe (Sea & Sun Technology GmbH, Trappenkamp, Germany) that included a turbidity (optical backscatter—OBS) sensor (Seapoint Sensors Inc., Exeter, NH, USA). The latter values were recorded in formazin turbidity units (FTU) [53].

At each measurement station, ~600 mL water samples were collected at ~30 cm below the water surface for subsequent SSC quantification in the laboratory. More than 180 water samples were analyzed. These samples were fractionated into subsamples, and their concentrations were determined through filtration [54]. The turbidity values were related to the SSC of the five studied estuaries through a quadratic polynomial correlation between concentrations of physical samples and measured FTU from the OBS sensor (suspended-sediment concentration, SSC (g·L^{-1}) = $0.0000008 \times (OBS)^2 + 0.0006 \times (OBS) + 0.0221$), $R^2 = 0.805$), and thus it was possible to convert turbidity data into SSC values (a scatter plot of this correlation is presented in the Figure S1).

The longitudinal CTD profiles for the estuaries of the Mocajuba, Taperaçu and Urumajó Rivers were conducted with vertical profiles spaced ~1 km apart along the estuaries. In the Caeté River estuary, the spacing was ~2 km. Because of the large extent of the Gurupi River in relation to the other estuaries, the spacing along the longitudinal profile was ~5 km.

3.2. Morphological Measurements, Tidal Amplitude, and Calculation of Tidal Prisms

In each of the five estuaries, bathymetric surveys were performed using a small boat and a Furuno 4100 echosounder (Furuno Electric Co., Ltd.—Nishinomiya, Japan) with dual frequencies of 50 and 200 kHz coupled to a Garmin 60CSx GPS (Garmin Ltd., Olathe, KA, USA). These devices were connected to a portable computer and the software standard data acquisition (SDA) v1.93 (Sea & Sun Technology GmbH, Trappenkamp, Germany) was used for the pairing and storage of the data obtained by the echo probe and the GPS. The data acquisition rate was 1 Hz, and the displacement speed of the boat oscillated between 1.5 and 2 m·s^{-1} (i.e., 3–4 knots). Each survey consisted of a series of cross-channel profiles and covered at least the distance from the limit of the saline intrusion upstream to the mouth of the estuary. The spacing between profiles ranged from 30 to 500 m, depending on the dimensions of the estuary.

To analyze the propagation and amplification of the tidal currents along the studied estuaries, digital tide gauges, model Onset/HOBO U20-002-Ti (Onset—Cape Cod, MA, USA), were installed at five points along the channel. Waterlevel variation along each

estuary was monitored in different periods and conditions, usually in week-long surveys, encompassing spring to neap tidal range, during low and high fluvial discharges (i.e., dry and rainy seasons). Bathymetric measurements were performed in all estuaries during intermediate fluvial discharge conditions, mainly around the high-water period of spring tides. To allow a proper comparison of the studied estuaries, we focused on the seasonal transition period at mean tidal-range conditions (intermediate between spring and neap), as datasets from these conditions were available for all five estuaries (a complete table summarizing periods and conditions of each measurement is provided as Table S1).

The water level variation data were then used to correct the bathymetric data. High-tide contours for each estuary were obtained from the shuttle radar topography mission (SRTM) data and satellite images. Morphological grids were prepared and maps and digital elevation models (DEMs) were generated using Surfer software (Golden Software LLC, Golden, CO, USA). We used the triangulation with linear-interpolation method and a spacing from 30 to 100 m, which was compatible with the acquisition of data and dimensions of each estuarine sector. The dynamic tide of each estuary was also analyzed, and the installation of the tide gauges aimed to detect the limit of upstream tide propagation. The contours of the river-estuarine channels were digitized from SRTM data and satellite images, and the depths of the thalweg were measured from longitudinal profiles when the tide gauges were installed. These data were also used for the generation of DEMs.

From the DEMs and the tide propagation in each estuary, we calculated the tidal prism, which is defined as the water volume between the mean low-tide and mean high-tide levels [55]. The mangrove areas in each estuary are extremely challenging for bathymetric and topographic surveys. However, these areas are only effectively flooded when the water level reaches ~2 m above the mean level, which only occurs during spring tides [20,42]. In the present study, the overall mean tidal range for the region was calculated to be 3.5 m and therefore mean tide is ~1.75 m and below the 2 m that would characterize overbank tides. Nevertheless, the mean spring tidal range is ~5 m, placing the region well within the macrotidal range. Thus, the tidal prisms were calculated based on the mean tide, according to the literature [11,55], avoiding the need and technical challenge of measuring the morphology and watershed limits of each estuary within the wide mangrove areas.

The tidal prisms were calculated in two distinct portions for each estuary. One comprised the main estuarine portion, which is affected by both the dynamic tide and the salt intrusion and corresponds to the middle and lower estuary. In this portion, detailed bathymetric surveys were performed, and the width of the channel reached up to 3 km. The second part comprises the high, upper estuary, where simplified bathymetric surveys were performed, including mostly longitudinal profiles along the thalweg and near each margin. There, the channel width was typically 20 to 50 m, and cross-sectional bathymetric profiles were not performed. This separation allowed one to make grids with adequate spacing for each portion, but also allowed a more detailed analysis of the tidal prism and of the role of the different river discharges and morphologies of each estuary.

4. Results and Discussion

4.1. SSC Distribution Patterns and Salinity

4.1.1. Regional Model of SSC Distribution and River Flow Rate Variations

As mentioned above, the distribution patterns of SSC and salinity of the Caeté River estuary (Figure 3) were initially evaluated as a starting point of the comparative analysis with other estuaries. A detailed analysis of the Caeté River estuary with respect to morphology, hydrodynamics, and suspended-sediment circulation has already been performed [20]. These results highlight the important combined role of flows during overbank tides (spring tides) and the direct impact of heavy monsoon rains during the first months of the year. The latter conditions greatly increase the SSC (Figure 3a–c). Additionally, offshore values of SSC are increased during that period [38,39], and this material is advected landwards due to estuarine circulation [20]. Overbank tides have similar effects in the dry season (Figure 3d–f). In both cases, increased values of SSCs are observed throughout the estuary,

although the synergistic effect of overbank tides on rainfall is strong [20]. In non-overbank (neap) tides (Figure 3g), SSCs are substantially less and much more localized, producing characteristic MTZs.
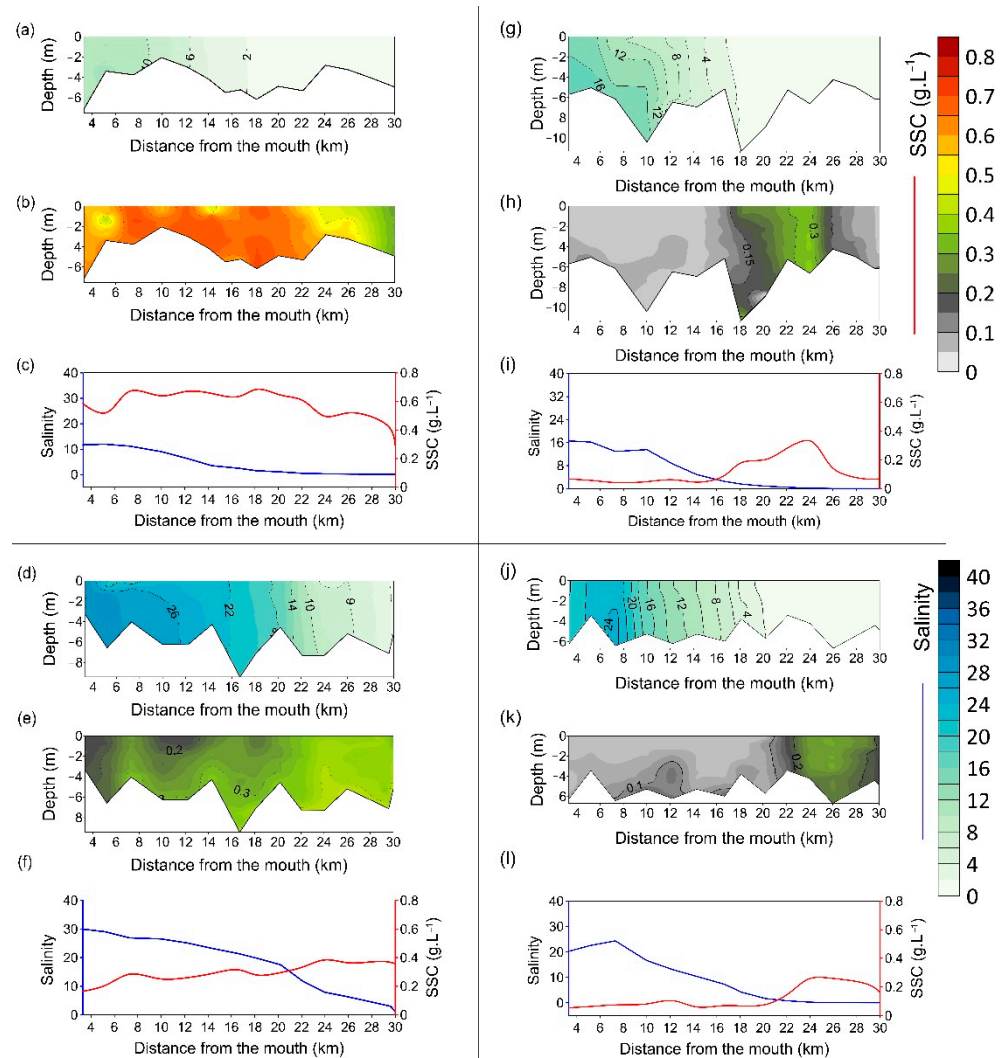

Figure 3. Longitudinal/vertical distribution patterns of salinity and suspended sediments at the Caeté estuary. Blue lines represent salinity, and red lines represent the SSC. Panels (**a**–**c**) represent the overbank tide condition during the rainy season; (**d**–**f**) represent overbank tides during the dry season; (**g**–**i**) represent non-overbank tides during the rainy season; and (**j**–**l**) represent the non-overbank tides during the dry season (modified from [20]).

Because the formation of the MTZ in tide-dominated estuaries is associated with transport convergence and is the product of the interaction between the river-tidal hydrodynamics and morphology [16], overbank tides significantly alter tide propagation in terms of morphology [20], which substantially contributes to the absence of distinct MTZs under these conditions. In turn, there is a clear displacement of the MTZ upstream (dry season) and downstream (rainy season), depending on the river discharge. Nevertheless, the MTZ always occurs at salinity values of 2 or less, as expected (e.g., Ref. [11]).

The results of this study show observed peaks in concentrations of suspended sediments occur in all of the five estuaries (Figure 4) investigated under non-overbank tide conditions and in the rainy season. When comparing the distribution of SSC, we find that the estuaries of the Urumajó River (small river discharge) and Gurupi River (large river discharge) exhibit a very similar pattern of MTZ formation to that of the Caeté River, and its positioning is consistent with the distribution of salinity (Figure 5). Data on overbank tides

in the case of the estuaries of the Urumajó and Gurupi Rivers also show similar patterns to those of the Caeté River, and the seasonal variations in the river discharge indicate the same displacement pattern of the MTZ.
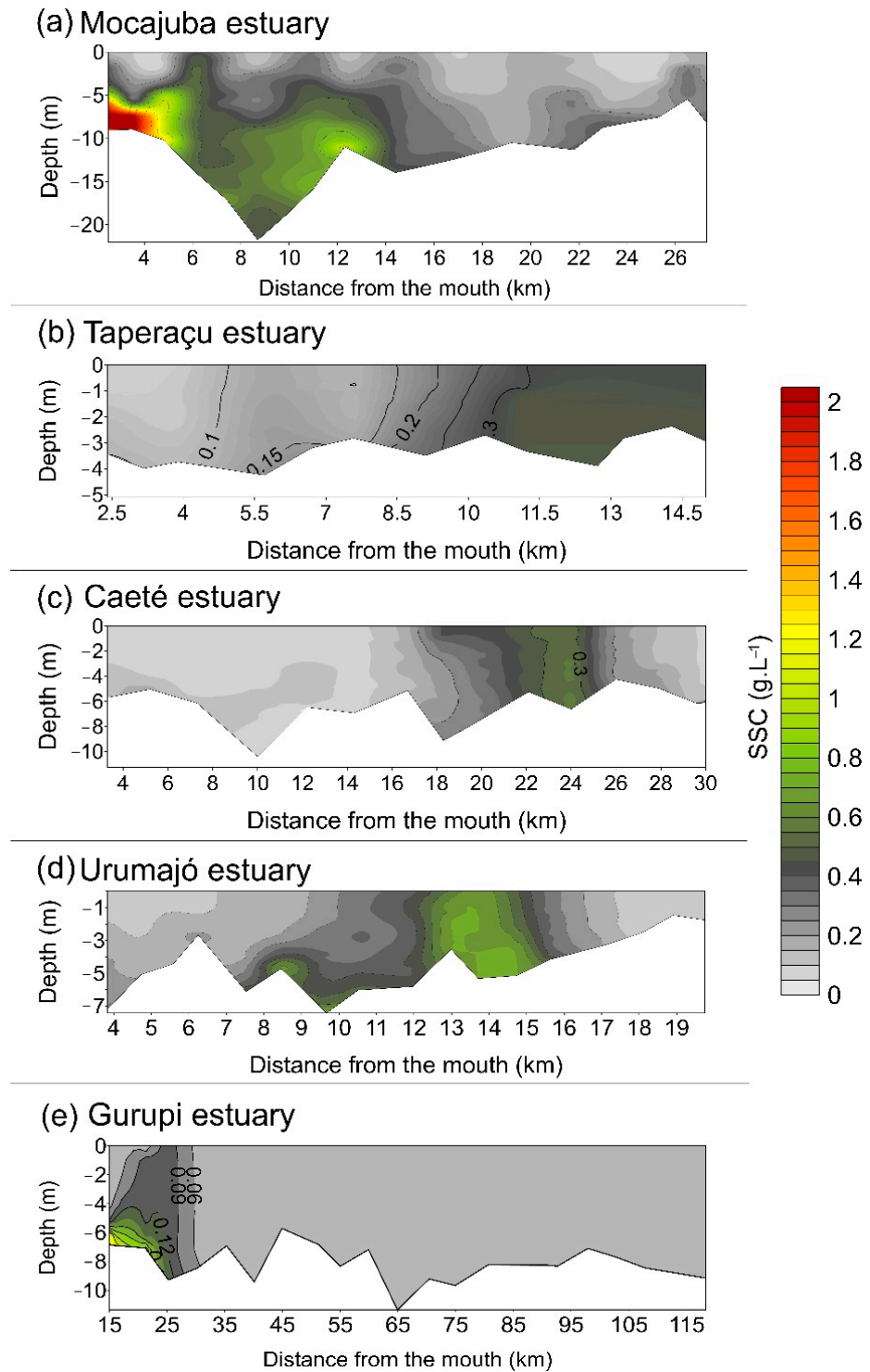

Figure 4. SSC distribution along the five estuaries during non-overbank tides of the rainy season (**a**) Mocajuba, (**b**) Taperaçu, (**c**) Caeté, (**d**) Urumajó, (**e**) Gurupi.
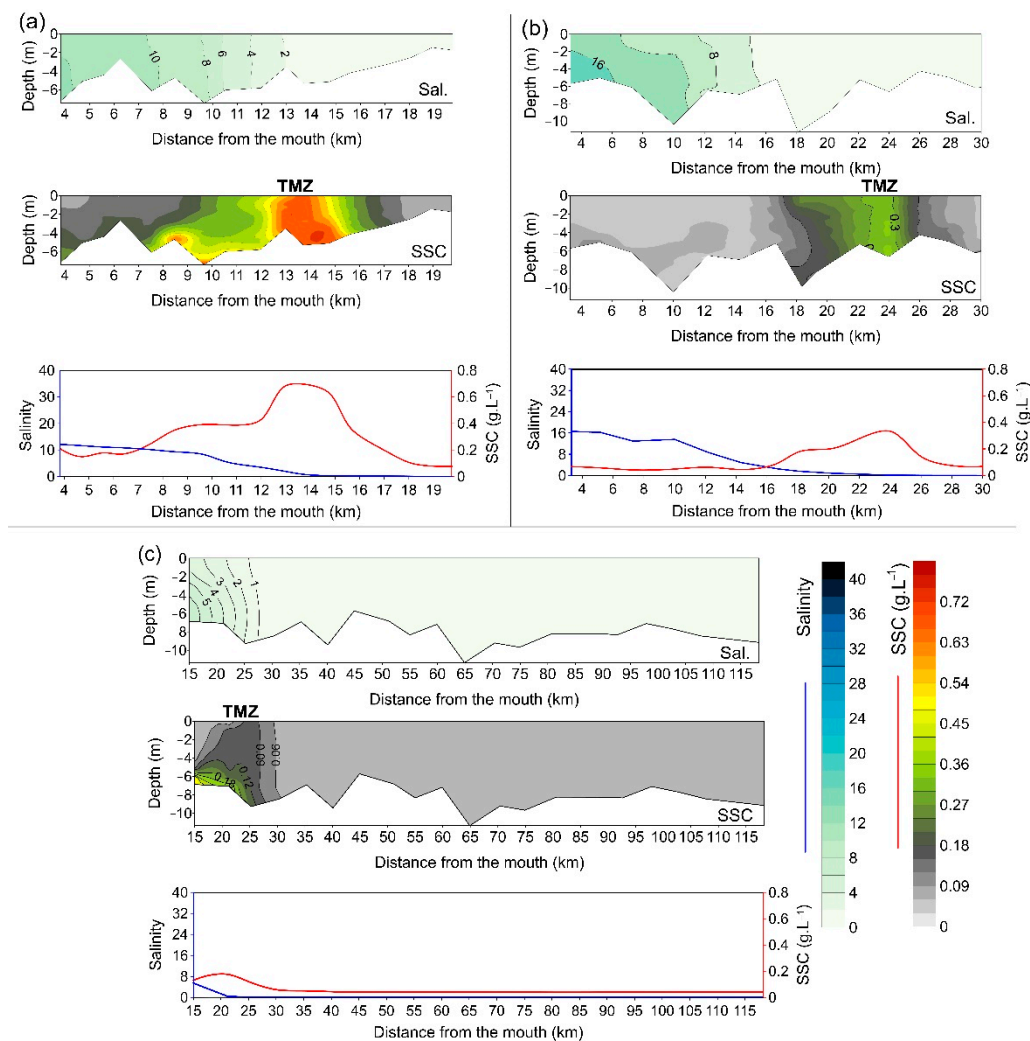
Figure 5. SSC and salinity distribution along the Urumajó (**a**), Caeté (**b**) and Gurupi (**c**) estuaries, during non-overbank tides of the rainy season. Blue lines represent salinity, and red lines represent the SSC. Salinity and SSC variations are coupled, and MTZ formation is evident.

In the case of the Mocajuba and Taperaçu estuaries, the variations diverged substantially from the pattern presented for the Caeté River estuary, although the data in non-overbank conditions and in the rainy season suggest the occurrence of an MTZ, as discussed below. Whereas the pattern of the Caeté includes an MTZ in the middle sector of the estuary, in association with the head of the salt intrusion, at the Mocajuba estuary the observed increased values of SSC are occurring near the estuarine mouth. On the other hand, at the Taperaçu estuary the increased SSC is observed in the upper sector. In both cases SSC is decoupled from salinity (Figure 6), with increased values of SSC occurring with salinities of ~32 (Mocajuba) or ~10 (Taperaçu).

When evaluating the longitudinal SSC distribution pattern during spring-tide conditions at the Caeté River estuary (Figure 3c), the effect of sediment resuspension by tidal currents results in high values of SSC in most of the estuarine length and from the bottom to the water surface, making MTZ delimitation and determination of location difficult [33]. During overbank tides there is still the transfer of suspended sediment from intertidal areas when the water level falls, causing the SSC in the estuarine channel to increase substantially. This discharge impacts estuarine hydrodynamics and the retention of fine sediment in the estuarine system [16,56].
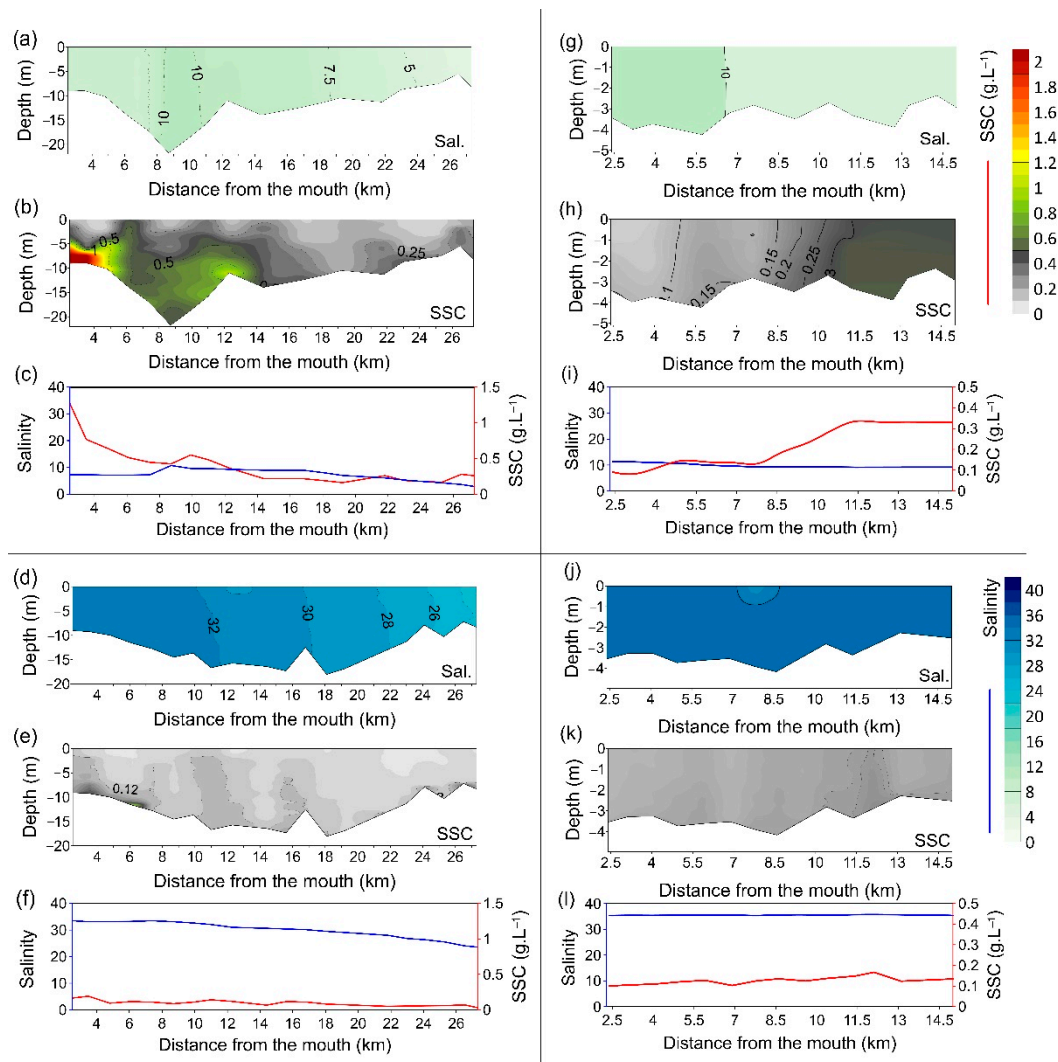
Figure 6. SSC and salinity distribution along the Mocajuba ((**a**–**c**) rainy season, (**d**–**f**) dry season) and Taperaçu ((**g**–**i**) rainy season, (**j**–**l**) dry season). Blue lines represent salinity and red lines represent the SSC. Notice that SSCs are substantially greater during the rainy season and that SSC and salinity variations are not clearly related.

This sensitivity of the location and values of SSC of the MTZ in tide-dominated estuaries to tidal range and river discharge is well known. For example, studies of four macrotidal estuarine systems in northern Europe (Weser, Seine, Scheldt, Humber) [24] and in six small estuarine systems in the central west coast of India [57], among others, have demonstrated this variation of SSC in the MTZ, as well as shifts in its position according to fluvial discharge variation. However, in all these cases, local rivers are the main source of SSC, whereas along the studied Amazon coastal sector the main source is offshore, which would correspond to the ARP in a long-term perspective [20].

4.1.2. Estuaries That Do Not Fit the Standard and Their Particularities

The comparison of suspended-sediment patterns between the Mocajuba and Taperaçu estuaries shows that increased concentrations occur only in the rainy season (Figure 6). In the Mocajuba River, there is a large concentration of suspended sediments in the outer/lower portion of the estuary, with an abrupt decrease upstream. In contrast, in the Taperaçu estuary the SSCs are minimal in the outer/lower portion and there is an increased concentration upstream (Figure 6). In both cases, the salinity distribution pattern suggests the variation in concentrations do not correspond to the formation of MTZ.

Other processes and factors can profoundly alter the distribution of suspended sediments in the estuaries of the eastern sector of the Amazon coastal zone, and here the connectivity between estuaries through tidal channels and the contribution of the Amazon River are particularly important [20,36,42–45,58]. In the case of the Taperaçu estuary, connectivity with the Caeté River estuary plays a predominant role in localized SSCs. In the case of the Mocajuba estuary, the connectivity or contribution of the Amazon River could be an important factor in the enhanced suspended-sediment concentration near the mouth (Figure 7).
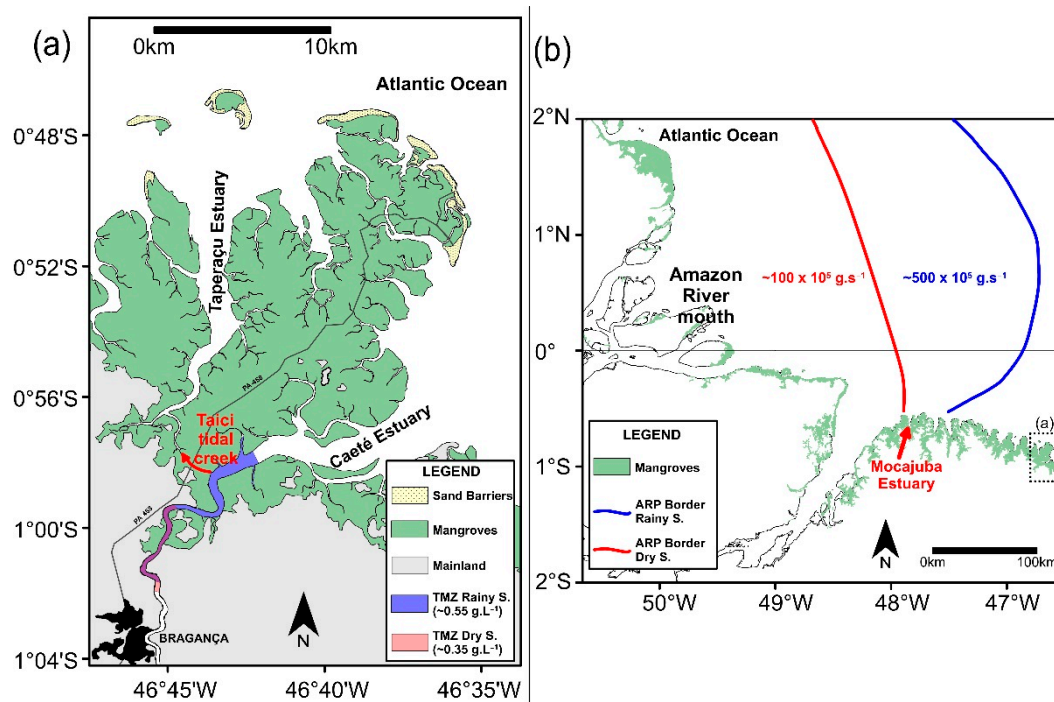

Figure 7. The seasonal displacement of the MTZ of the Caeté estuary [20] and the location of the Furo do Taici tidal creek are shown in (**a**). Seasonal displacement of the Amazon River plume (ARP) [25] is shown in (**b**) where the presented values correspond to seasonal SSC plume discharge according to [43]. In both cases the position and concentrations of the primary suspended-sediment source for the Mocajuba estuary (i.e., the ARP) and for the Taperaçu estuary (i.e., the Caeté MTZ) explain observed concentrations showed in Figure 6.

When evaluating the seasonal variation in the SSC distribution in the Taperaçu estuary, we note that the pattern of greater concentration up-estuary is correlated with the seasonal location of the MTZ of the Caeté estuary. The suspended sediments of the latter are carried to the Taperaçu estuary through a connection channel (Furo do Taici) [20,42,43], and this process is favored during the rainy season. This is due to the position of the MTZ in the area of the Furo do Taici and by the higher concentrations during this period (Figure 7a).

Among the cases studied, the Mocajuba River is the closest to the mouth of the Amazon River and therefore the most susceptible to the effect of its plume. It has been demonstrated that the seasonal plume variations, especially due to the seasonal variation in the direction and intensity of the winds, strongly affect the area during the rainy season [38,39]. The comparison between the seasonal variation in the suspended-sediment distribution pattern in the Mocajuba River and the mean seasonal position of the Amazon River plume highlights this seasonal contribution and explains the decrease in SSC upstream, because in this case there is a substantial input from offshore, resulting in substantially increased values of SSC at the lower Mocajuba estuary, which abruptly decrease in the upstream direction (Figure 6). This occurs especially during the first half of the year, when the ARP is more sediment-laden at the Mocajuba estuarine mouth (Figure 7b). For all five investigated estu-

aries there is a mud supply from offshore, probably related with the ARP [20,35], but there is a strong eastward decreasing gradient of this supply, with the distance from the Amazon River mouth, so that its effect is most conspicuous at the Mocajuba estuary (Figure 7b).

These results indicate that while the estuaries of Caeté, Urumajó and Gurupi have typical MTZs for tide-dominated estuaries, the Mocajuba and Taperaçu do not have distinct MTZs, although seasonally localized increased SSCs are observed. Within this study, an MTZ is defined as a distinct estuarine zone with perennial increased values of SSC as a result of transport convergence occurring at, or near to, the head of the salt intrusion [11,17], which is not the case for the Mocajuba and Taperaçu estuaries. In those cases, the different morphology and proximity to the Amazon River plume of the Mocajuba estuary and the absence of river discharge in the Taperaçu estuary explain their absence of MTZs, where observed increased SSC zones are only seasonal, and not related with the head of the salt intrusion or the sediment transport convergence.

We hypothesize that the reason for MTZ absence in the Mocajuba and Taperaçu estuaries lies with their geomorphic characteristics. To assess this, the morphology of Taperaçu and Mocajuba estuaries was compared with the morphology of the Urumajó estuary, which has an MTZ and has dimensions comparable to the other two estuaries, allowing a proper comparison. From the developed DEMs several cross-sections were extracted from each estuary, with a 1–2 km spacing, composing a longitudinal profile of the channel geometry (Figure 8). These profiles extend upstream to the limit of salt intrusion.

Considering the cross-sectional area (Figure 8a), Taperaçu and Urumajó estuaries are similar, exhibiting a funnel-shaped seaward portion with substantial upstream convergence, whereas the Mocajuba estuary stands out with a substantially greater cross-sectional area along the entire evaluated extent. Considering the relationship of the channel width and channel depth for each cross-section (Figure 8b), the Taperaçu estuary stands out, being substantially shallower than the Urumajó and Mocajuba estuaries. On the other hand, while comparing the local cross-section depth (h) with the mean tidal range (a), all three estuaries can be discerned (Figure 8c). The Mocajuba is deep in relation to the tidal range (average a/h = 0.442) and the Taperaçu is shallow (average a/h = 1.081), with the Urumajó estuary representing an average equilibrium condition (a/h = 0.769).

4.2. Interaction of Channel Morphology and Tidal Propagation and Its Control of SSC Patterns

Effects of the geomorphology on tidal propagation are largely discussed in the scientific literature for estuaries around the world (e.g., Refs. [13–15,59–61]), as well as along the Amazon coast (e.g., Refs. [1,20,35,36,42,58]). When ocean tides propagate into shallow estuaries, they are modified and thus produce a landward or seaward residual transport [18]. Three main distinct processes are recognized: (1) frictional damping on the bottom; (2) landward constriction or convergence in the channel; and (3) reflection on shoals or at the estuary head [60]. For tide-dominated estuaries the balance between friction and convergence is particularly relevant [16].

Nevertheless, as early recognized for coastal environments such as estuaries mostly formed by unconsolidated sediments [62], the interaction and feedback between the morphology and hydrodynamics define sediment transport pathways and subsequent morphodynamic evolution. Therefore, we assume that the assessment of tidal prism and tidal wave modification along an estuary is a simple and effective way to investigate the interaction of morphology and dynamics, in terms not only of the tidal propagation but also in consideration of fluvial discharge effects.

A detailed analysis of the tidal prisms and volumes of the channels in each of the five estuaries was conducted to evaluate the interaction between channel morphology and tidal propagation in the control of SSC patterns (Table 2). The results for the distribution of the SSC and salinity indicate a group of typical estuaries, although showing a substantial range of local river flow rates, from the Urumajó (mean flow rate of 10 $m^3 \cdot s^{-1}$) to the Caeté (mean flow rate of 41.5 $m^3 \cdot s^{-1}$) to the Gurupi (mean flow rate of 472 $m^3 \cdot s^{-1}$). These estuaries have perennial river flow rates (Table 1), which causes substantial effect on salinity variation

(Figure 5). They also exhibit a tidal prism typically between $\frac{1}{2}$ and $\frac{2}{3}$ of the total estuary volume (Table 2, Figure 9).
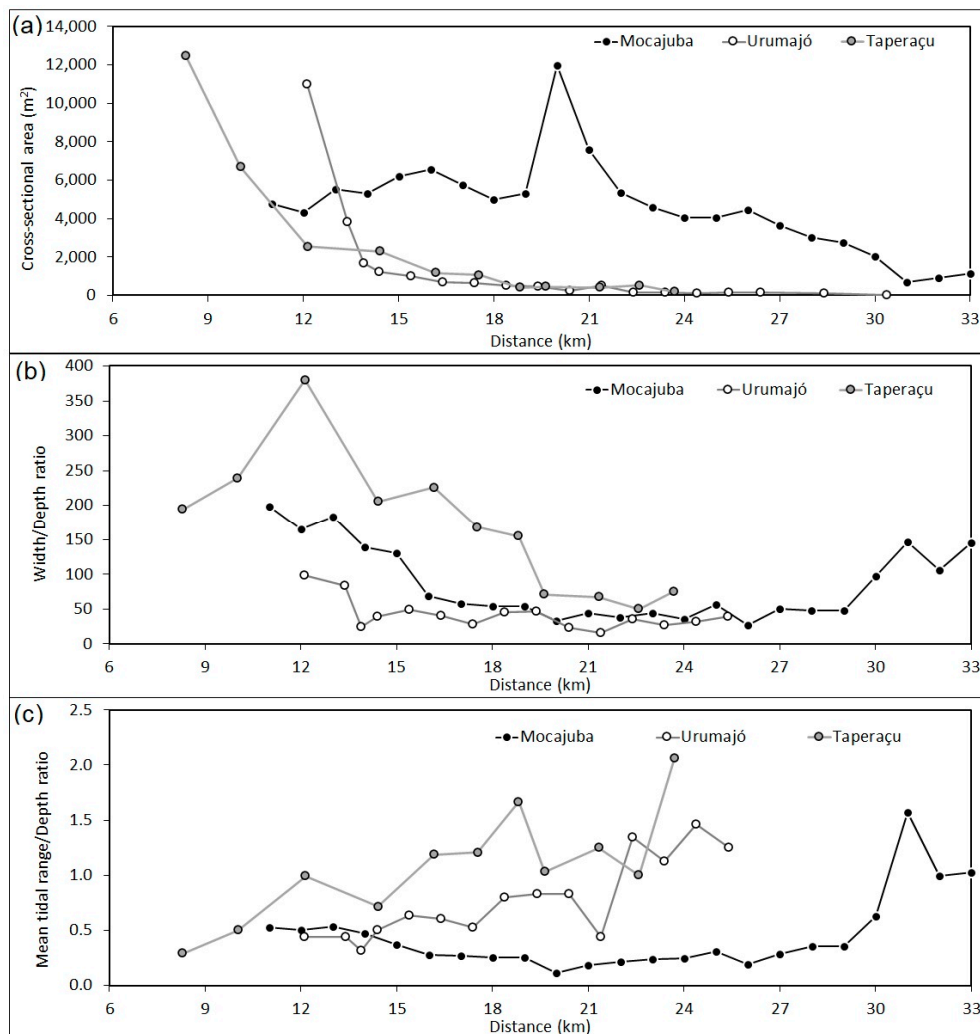

Figure 8. Comparison of geomorphic characteristics of the Mocajuba, Taperaçu and Urumajó estuaries considering the longitudinal variation from the estuarine mouth of the cross-sectional area (**a**), the relationship of the channel width and channel depth (**b**) and the ratio of the mean tidal range with the local cross-section depth (**c**).

Table 2. Tidal prism and channel volume calculations ($\times 10^{12}$ m³, three significant figures) for the five evaluated estuaries. Note that all volumes are presented for the entire estuary (total), as well as separately for the portion from the mouth up to the salt-intrusion limit (salt estuary) and the portion of the upper estuary from the salt-intrusion limit to the tide limit upstream (tidal river).

| Section		Mocajuba	Taperaçu	Caeté	Urumajó	Gurupi
Total	Total vol. [1]	14.5	5.49	51.6	28.0	75.677
	Channel vol. [1]	8.29	1.03	17.4	9.10	31.09
	Tidal prism [1]	6.22	4.46	34.1	18.9	44.587
Salt estuary	Total vol. [1]	14.4	5.49	50.7	27.9	71.413
	Channel vol. [1]	8.27	1.03	17.2	9.08	28.594
	Tidal prism [1]	6.09	4.46	33.6	18.8	42.819
Tidal river	Total vol. [1]	0.16	0	0.82	0.07	4.2634
	Channel vol. [1]	0.03	0	0.24	0.03	2.4957
	Tidal prism [1]	0.13	0	0.59	0.04	1.7678
	Relat. prism	2.12%	0.00%	1.75%	0.24%	4.13%

[1] $\times 10^{12}$ m³.
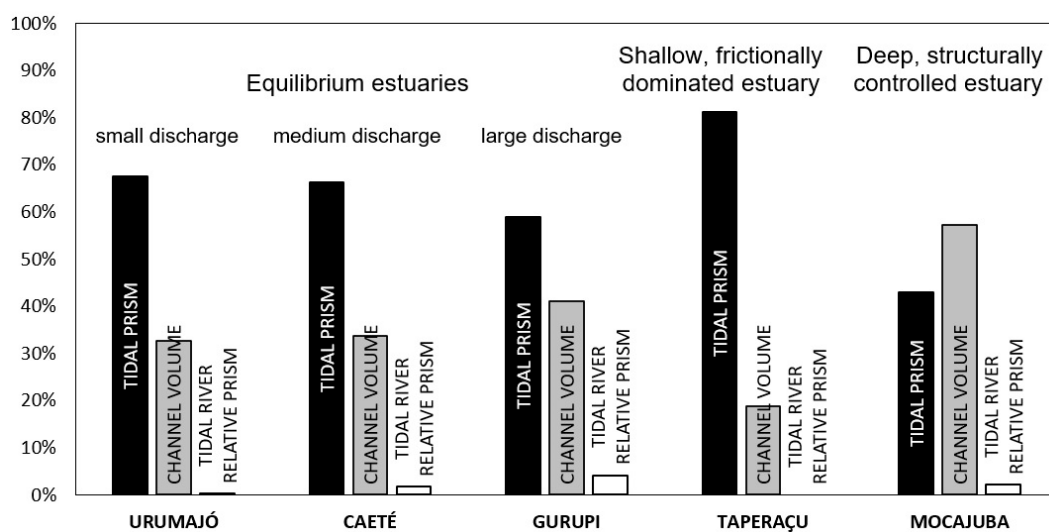
Figure 9. Tidal-prism and channel volumes for the investigated estuaries, showing the effect of the river discharge increase, within the proportion of the tidal prism represented by the given tidal-river portion (the first three from the left). Note that Taperaçu and Mocajuba estuaries also have morphological peculiarities.

The data show that the tidal prism represents most of the total volume, although the greater the river flow rate, the greater the channel volume represents of the total volume, as expected. For the Urumajó, Caeté and Gurupi estuaries, the tidal prism represents 68%, 66% and 59% of the total volume, respectively. Additionally, the relative volume of the tidal prism in the upper portion of the estuary, beyond the saline intrusion, gradually increases with the relative magnitude of the river flow rate, and it corresponds to 0.2% for Urumajó (drainage 544 km^2, 10 m$^3 \cdot$s^{-1}), 1.8% for Caeté (2240 km^2, 41.5 m$^3 \cdot$s^{-1}) and 4.1% for Gurupi (~35,000 km^2, 472 m$^3 \cdot$s^{-1})—all below the 5% of the total tidal prism volume seen in each estuary. Considering these characteristics, it is considered that these estuaries present an equilibrium between morphology and hydrodynamics, and are therefore called equilibrium estuaries (Table 2, Figure 9).

The other estuaries investigated (i.e., Taperaçu and Mocajuba) have tidal dimensions comparable to that of the Urumajó River (Figure 9). When compared to the latter, the Taperaçu estuary has a large proportion of its volume (>80%) corresponding to the tidal prism. In turn, the estuary of the Mocajuba River has a tidal prism proportion of only ~43% (Figure 9).

It has been shown that the Taperaçu estuary is very shallow and frictionally dominated because of the absence of a perennial river discharge and a flood-dominated sediment transport. Consequently, these conditions are responsible for the advanced state of infilling [42]. Although the gradual infilling might result in a change from flood- to ebb-dominant flow [13], strongly flood-dominated systems are unlikely to evolve into ebb-dominated systems by the action of a persistent offshore tide [14]. Current measurements at different points along the Taperaçu estuary show consistent flood-dominance [42]. In addition, the consistent landward reduction in tidal range along the Taperaçu estuary reflects that frictional effects overcome convergence effects, as the large channel width-depth ratio (Figure 8b) and tidal range-depth ratio (Figure 8c) suggest.

In the case of the Mocajuba River, the bathymetric surveys of the present study, which corroborate early work [36], reveal its substantial depth, which has been attributed to structural control and neotectonics in the region [1,36,63]. Current measurements in a cross-section in the middle sector of the Mocajuba estuary [36] have shown an ebb-dominant pattern, in agreement with its morphological characteristics, especially the significantly larger cross-sectional area (Figure 8a). Current measurements also show

velocity magnitudes half as large as those observed in any other investigated estuary, reflecting its inherited deeper and wider morphology (Figure 8). The morphological and hydrodynamic characteristics of the estuaries Taperaçu and Mocajuba—here represented by the volumes of the tidal prisms, channels, and tidal river portion of each estuary— contribute to the explanation of the absence of MTZs in these estuaries (Figure 9).

The presented analysis of tidal prism and channel volumes (Figure 9) clearly reflects the interplay between tidal propagation and morphology. It has been demonstrated that water level and current velocity variations along estuaries follow consistent patterns as a result of the balance between frictional and convergence effects [18]. Besides, water level variations are easily correlated to the morphology in terms of tidal prism evaluation, whereas the evaluation of geomorphic effects on currents are more complex and require longitudinally representative measurements for all five evaluated systems, which are not available. Therefore, we present a comprehensive comparison of tidal propagation along the five estuaries (Figure 10).
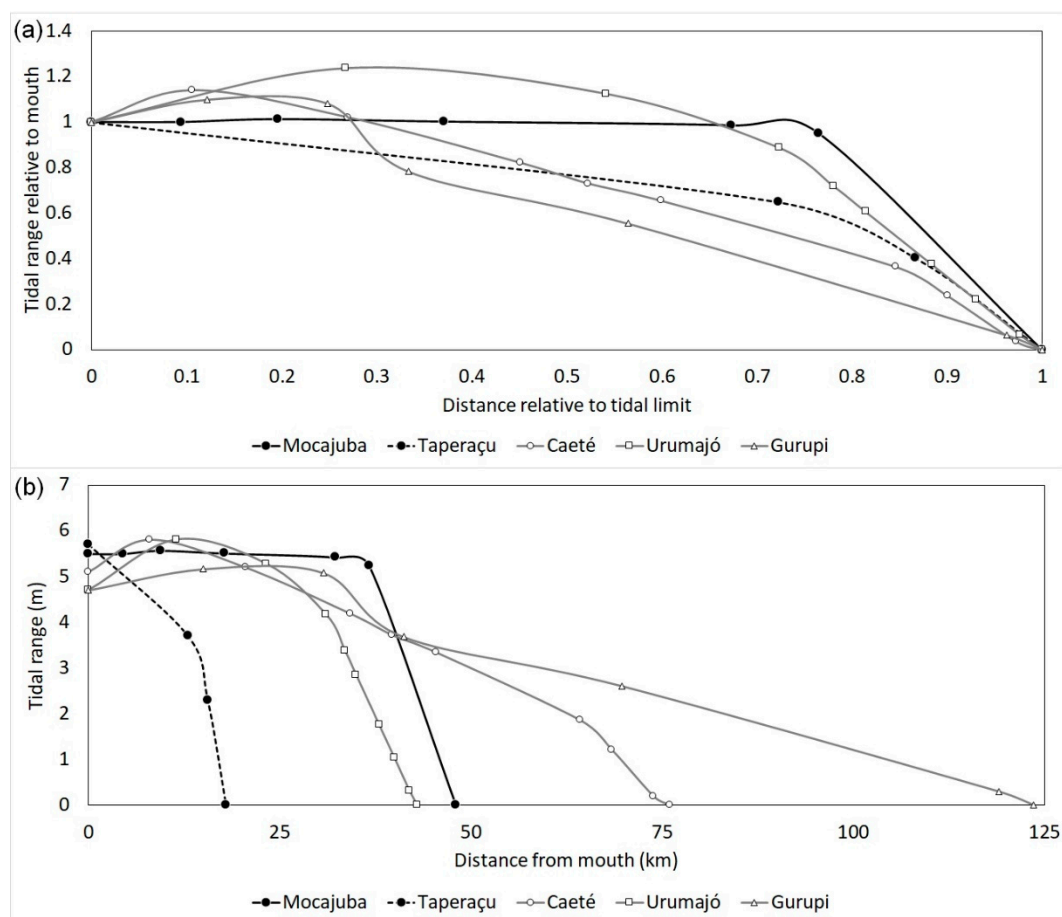
Figure 10. Tidal propagation along the five evaluated estuaries. Tidal ranges and distances are presented in relative proportions (**a**) and absolute values (**b**). Urumajó, Caeté and Gurupi estuaries show a hypersynchronous pattern, whereas the Taperaçu estuary is hyposynchronous and the Mocajuba estuary is synchronous.

The morphology has a great influence on the dynamics and retention of fine sediments along the estuaries. It controls the propagation of tidal waves and the formation and location of MTZ in the estuary, besides other factors such as fluvial discharge. Nevertheless, substantial differences in fluvial discharge (Figure 9) show a substantially smaller impact on tidal propagation (Figure 10) in comparison to their geomorphic characteristics. Most of the estuaries show hypersynchronous behavior, where at first the convergence effect overcomes the friction effect and there is an amplification of the tide before it decays upstream due

to frictional effects (Figure 10). However, the Taperaçu estuary, which is frictionally dominated, presents hyposynchronous behavior with a continuous landward decline in tidal amplitude (Figure 10). Additionally, the Mocajuba estuary shows synchronous behavior, where large cross-sectional areas cause the effects of convergence and friction to be very reduced. The tide propagates without amplification or significant attenuation along most of its length, finally becoming attenuated in the tidal-river portion of the system (Figure 10). These behaviors impact the degree of tidal pumping and convergence of sediment in an MTZ.

Observations in numerous estuaries [16,18] demonstrate that increased values of SSC are not necessarily associated with the limit of the salt intrusion or propagation of the tides, but associated with the bathymetric characteristics of the estuaries. Herewith such concentrations are not referred to as MTZs. This relationship also occurs in the northern San Francisco Bay [64], the Columbia River [65], the Delaware River [66], the Chesapeake Bay [67] and the Elbe River [68].

The analysis of the tidal amplitude, amplitude ratio and phase relationship for the M2 and M4 tidal constituents along the Caeté estuary [20] shows the longitudinal transport convergence coinciding with the sector of maximum tidal range (Figure 10). This pattern is also assumed for Urumajó and Gurupi estuaries, and would characterize the hypersynchronous, equilibrium estuaries.

Results show that the Taperaçu and Mocajuba estuaries do not have MTZs, although they have discrete areas of seasonally increased values of SSC (Figures 6 and 7). These estuaries show an unbalanced condition between flow and morphology, which is the product of inherited morphology for the Mocajuba, and lack of fluvial discharge for the Taperaçu estuary [42]. It highlights other processes that are relevant to the suspended-sediment dynamics at the regional level, i.e., the contribution of the Amazon River plume (ARP) and the role of connectivity between estuaries. While the SSC supply from the ARP decreases eastwards, connective tidal channels redistribute part of these fine-grained sediments between estuaries [20,45].

5. Concluding Remarks

Based on data collected in five estuarine systems of the southeastern Amazon coast, the relationship between suspended-sediment dynamics, the MTZ formation and morphology of the systems has been demonstrated. Vertical circulation, tidal pumping, and resuspension are identified as the main mechanisms that control SSC in tide-dominated estuaries [17]. These mechanisms result in sediment transport convergence and consequently in MTZ formation [11]. This study reinforces this for estuaries with a broad range of fluvial discharges, as long as their morphology is in an equilibrium state with the modern hydrodynamics.

The differences in tidal propagation as a function of the morphology of each estuary differentiate them as hypersynchronous (Urumajó, Caeté, Gurupi), synchronous (Mocajuba) and hyposynchronous (Taperaçu). This determines the relative balance between river flow rate, friction and depth, controlling their behavior and potential for tidal pumping. The estuaries of Caeté, Urumajó and Gurupi Rivers have typical MTZs for tide-dominated estuaries, and the Mocajuba and Taperaçu estuaries do not have distinct MTZs, although localized concentrations are observed seasonally. In this case, the non-equilibrium morphology of the Mocajuba estuary and the absence of river discharge in the Taperaçu estuary explain their absences of MTZs.

The behavior of estuaries subjected to similar external forcing conditions but with different morphologies document the importance of morphology in the control of MTZ dynamics. Understanding the MTZs of estuaries not only has theoretical importance regarding the mechanisms involved, but also has relevance to understanding aspects related to the sedimentation, ecology and biogeochemistry of estuarine systems. This study identifies the trapping of SSC discharged by the Amazon River in the MTZs of

estuaries along the southeastern Amazon coast, which substantially contributes to the longest continuous mangrove belt of the world.

References

1. Lessa, G.C.; Santos, F.M.; Souza Filho, P.W.; Corrêa-Gomes, L.C. Brazilian estuaries: A geomorphologic and oceanographic perspective. In *Brazilian Estuaries. Brazilian Marine Biodiversity*; Lana, P., Bernardino, A., Eds.; Springer: Cham, Switzerland, 2018; pp. 1–37.
2. Fairbridge, R.W. The estuary: Its definition and geodynamic cycle. In *Chemistry and Biogeochemistry of Estuaries*; Olausson, E., Cato, I., Eds.; John Wiley and Sons Ltd.: New York, NY, USA, 1980; pp. 1–35.
3. Dalrymple, R.W.; Zaitlin, B.A.; Boyd, R. Estuarine facies models: Conceptual basis and stratigraphic implications. *J. Sediment. Petrol.* **1992**, *62*, 1130–1146. [CrossRef]
4. Boyd, R.; Dalrymple, R.; Zaitlin, B.A. Classification of clastic coastal depositional environments. *Sediment. Geol.* **1992**, *80*, 139–150. [CrossRef]
5. Pritchard, D.W. Estuarine Hydrography. *Adv. Geophys.* **1952**, *1*, 243–280. [CrossRef]
6. Cameron, W.M.; Pritchard, D.W. Estuaries. In *The Sea: Ideas and Observations on Progress in the Study of the Seas*; Hill, M.N., Ed.; Wiley: New York, NY, USA, 1963; pp. 306–324.
7. Pritchard, D.W. What is an Estuary: Physical Viewpoint? In *Estuaries*; Lauff, G.H., Ed.; American Association for the Advancement of Science: Washington, DC, USA, 1967; pp. 3–5.
8. Caspers, H. Estuaries: Analysis of Definitions and Biological Considerations. In *Estuaries*; Lauff, G.H., Ed.; American Association for the Advance of Science: Washington, DC, USA, 1967; pp. 6–8.
9. Hansen, D.V.; Rattray, M. New dimensions in estuary classification. *Limnol. Oceanogr.* **1966**, *11*, 319–326. [CrossRef]
10. Ibañez, C.; Pont, D.; Prat, N. Characterization of the Ebre and Rhone estuaries: A basis for defining and classifying salt-wedge estuaries. *Limnol. Oceanogr.* **1997**, *42*, 89–101. [CrossRef]
11. Dyer, K.R. *Estuaries: A Physical Introduction*, 2nd ed.; John Wiley and Sons Ltd.: New York, NY, USA, 1997; ISBN 0-471-9741-4.
12. Chappell, J.; Woodroffe, C. Macrotidal estuaries. In *Coastal Evolution: Late Quaternary Shoreline Morphodynamics*; Carter, R.W., Woodroffe, C.D., Eds.; Cambridge University Press: Cambridge, UK, 1994; pp. 187–218.

13. Boon, J.D.; Byrne, R.J. On basin hyposmetry and the morphodynamic response of coastal inlet systems. *Mar. Geol.* **1981**, *40*, 27–48. [CrossRef]

14. Friedrichs, C.T.; Aubrey, D.G. Nonlinear tidal distortion in shallow well-mixed estuaries. *Estuar. Coast. Shelf Sci.* **1988**, *27*, 521–545. [CrossRef]

15. Lessa, G.; Masselink, G. Morphodynamic evolution of a macrotidal barrier estuary. *Mar. Geol.* **1995**, *129*, 25–46. [CrossRef]

16. Burchard, H.; Schuttelaars, H.M.; Ralston, D.K. Sediment trapping in estuaries. *Ann. Rev. Mar. Sci.* **2018**, *10*, 371–395. [CrossRef] [PubMed]

17. Dyer, K.R. Sediment transport processes in estuaries. In *Developments in Sedimentology*; Perillo, G.M.E., Ed.; Elsevier Science: Oxford, UK, 1995; Volume 53, pp. 423–449.

18. Nichols, M.M.; Biggs, R.B. Estuaries. In *Coastal Sedimentary Environments*; Davis, R.A., Jr., Ed.; Springer: New York, NY, USA, 1985; pp. 77–186.

19. Van Maanen, B.; Sottolichio, A. Hydro- and sediment dynamics in the Gironde estuary (France): Sensitivity to seasonal variations in river inflow and sea-level rise. *Cont. Shelf Res.* **2018**, *165*, 37–50. [CrossRef]

20. Asp, N.E.; Gomes, V.J.C.; Schettini, C.A.F.; Souza-Filho, P.W.M.; Siegle, E.; Ogston, A.S.; Nittrouer, C.A.; Silva, J.N.S.; Nascimento, W.R.; Souza, S.R.; et al. Sediment dynamics of a tropical tide-dominated estuary: Turbidity maximum, mangroves and the role of the Amazon River sediment load. *Estuar. Coast. Shelf Sci.* **2018**, *214*, 10–24. [CrossRef]

21. Capo, S.; Sottolichio, A.; Brenon, I.; Castaing, P.; Ferry, L. Morphology, hydrography and sediment dynamics in a mangrove estuary: The Konkoure Estuary, Guinea. *Mar. Geol.* **2006**, *230*, 199–215. [CrossRef]

22. Jiang, X.; Lu, B.; He, Y. Response of the turbidity maximum zone to fluctuations in sediment discharge from river to estuary in the Changjiang Estuary (China). *Estuar. Coast. Shelf Sci.* **2013**, *131*, 24–30. [CrossRef]

23. Gong, W.; Jia, L.; Shen, J.; Liu, J.T. Sediment transport in response to changes in river discharge and tidal mixing in a funnel-shaped micro-tidal estuary. *Cont. Shelf Res.* **2014**, *76*, 89–107. [CrossRef]

24. Uncles, R.J.; Stephens, J.A. Distributions of suspended sediment at high water in a macrotidal estuary. *J. Geophys. Res. Ocean.* **1989**, *94*, 14395–14405. [CrossRef]

25. Azhikodan, G.; Yokoyama, K. Spatio-temporal variability of phytoplankton (Chlorophyll-a) in relation to salinity, suspended sediment concentration, and light intensity in a macrotidal estuary. *Cont. Shelf Res.* **2016**, *126*, 15–26. [CrossRef]

26. Azhikodan, G.; Yokoyama, K. Erosion and sedimentation pattern of fine sediments and its physical characteristics in a macrotidal estuary. *Sci. Total Environ.* **2021**, *753*, 142025. [CrossRef]

27. McAnally, W.H.; Friedrichs, C.; Hamilton, D.; Hayter, E.; Shrestha, P.; Rodriguez, H.; Sheremet, A.; Teeter, A. Management of fluid mud in estuaries, bays, and lakes. I: Present state of understanding on character and behavior. *J. Hydraul. Eng.* **2007**, *133*, 9–22. [CrossRef]

28. Shen, H.T.; He, S.L.; Pan, D.A.; Li, J.F. A study of turbidity maximum in the Changjiang estuary. *Acta Geogr. Sin.* **1992**, *47*, 472–479.

29. Yu, Q.; Wang, Y.; Gao, J.; Gao, S.; Flemming, B. Turbidity maximum formation in a well-mixed macrotidal estuary: The role of tidal pumping. *Geophys. Res. Ocean.* **2014**, *119*, 7705–7724. [CrossRef]

30. Doxaran, D.; Castaing, P.; Lavender, S.J. Monitoring the maximum turbidity zone and detecting fine-scale turbidity features in the Gironde estuary using high spatial resolution satellite sensor (SPOT HRV, Landsat ETM+) data. *Int. J. Remote. Sens.* **2006**, *27*, 2303–2321. [CrossRef]

31. Uncles, R.J.; Stephens, J.A.; Harris, C. Runoff and tidal influences on the estuarine turbidity maximum of a highly turbid system: The upper Humber and Ouse Estuary, UK. *Mar. Geol.* **2006**, *235*, 213–228. [CrossRef]

32. Mitchell, S.B. Turbidity maxima in four macrotidal estuaries. *Ocean Coast. Manag.* **2013**, *79*, 62–69. [CrossRef]

33. Asp, N.E.; Gomes, V.J.C.; Ogston, A.; Borges, J.C.C.; Nittrouer, C.A. Sediment source, turbidity maximum, and implications for mud exchange between channel and mangroves in an Amazonian estuary. *Ocean Dyn.* **2016**, *66*, 285–297. [CrossRef]

34. Nascimento, W.R.; Souza-Filho, P.W.M.; Proisy, C.; Lucas, R.M.; Rosenqvist, A. Mapping changes in the largest continuous Amazonian mangrove belt using object-based classification of multisensor satellite imagery. *Estuar. Coast. Shelf Sci.* **2013**, *117*, 83–93. [CrossRef]

35. Souza-Filho, P.W.M.; Lessa, G.C.; Cohen, M.C.L.; Costa, F.R.; Lara, R.J. The subsiding macrotidal barrier estuarine system of the Eastern Amazon Coast, Northern Brazil. In *Geology and Geomorphology of Holocene Coastal Barriers of Brazil*; Lecture Notes in Earth Sciences; Springer: Berlin/Heidelberg, Germany, 2009; Volume 107, pp. 347–375; ISBN 9783540250081.

36. Asp, N.E.; Amorim de Freitas, P.T.; Gomes, V.J.C.; Gomes, J.D. Hydrodynamic overview and seasonal variation of estuaries at the eastern sector of the Amazonian coast. *J. Coast. Res.* **2013**, *165*, 1092–1097. [CrossRef]

37. Meade, R.H.; Dunne, T.; Richey, J.E.; Santos, U.D.M.; Salati, E. Storage and remobilization of suspended sediment in the lower Amazon River of Brazil. *Science* **1985**, *228*, 488–490. [CrossRef] [PubMed]

38. Nittrouer, C.A.; Kuehl, S.A.; Sternberg, R.W.; Figueiredo, A.G.; Faria, L.E.C. An introduction to the geological significance of sediment transport and accumulation on the Amazon continental shelf. *Mar. Geol.* **1995**, *125*, 177–192. [CrossRef]

39. Geyer, W.R.; Beardsley, R.C.; Lentz, S.J.; Candela, J.; Limeburner, R.; Johns, W.E.; Castro, B.M.; Soares, I.D. Physical oceanography of the Amazon shelf. *Cont. Shelf Res.* **1996**, *16*, 575–616. [CrossRef]

40. Gomes, V.J.C.; Freitas, P.T.A.; Asp, N.E. Dynamics and seasonality of the middle sector of a macrotidal estuary. *J. Coast. Res.* **2013**, *165*, 1140–1145. [CrossRef]

41. ANA—Agência Nacional de Águas Hidroweb: Serviço de Informações Hidrológicas. Available online: http://www3.ana.gov.br (accessed on 12 December 2020).
42. Asp, N.E.; Schettini, C.A.F.; Siegle, E.; da Silva, M.S.; de Brito, R.N.R. The dynamics of a frictionally-dominated Amazonian estuary. *Braz. J. Oceanogr.* **2012**, *60*, 391–403. [CrossRef]
43. Araújo, W.P., Jr.; Asp, N.E. Hydrodynamic connectivity between two macrotidal Amazonian estuaries. *J. Coast. Res.* **2013**, *65*, 1086–1091. [CrossRef]
44. McLachlan, R.L.; Ogston, A.S.; Asp, N.E.; Fricke, A.T.; Nittrouer, C.A.; Gomes, V.J.C. Impacts of tidal-channel connectivity on transport asymmetry and sediment exchange with mangrove forests. *Estuar. Coast. Shelf Sci.* **2020**, *233*, 106524. [CrossRef]
45. Gomes, V.J.C.; Asp, N.E.; Siegle, E.; McLachlan, R.L.; Ogston, A.S.; Silva, A.M.M.; Nittrouer, C.A.; Souza, D.F. Connection between macrotidal estuaries along the southeastern Amazon coast and its role in coastal progradation. *Estuar. Coast. Shelf Sci.* **2020**, *240*, 106794. [CrossRef]
46. Magalhães, A.; Pereira, L.C.C.; da Costa, R.M. Relationships between copepod community structure, rainfall regimes, and hydrological variables in a tropical mangrove estuary (Amazon coast, Brazil). *Helgol. Mar. Res.* **2015**, *69*, 123–136. [CrossRef]
47. Martins, E.S.F.; Souza, F.P.W.M.; Costa, F.R.; Alves, P.J.O. Extração automatizada e caracterização da rede de drenagem e das bacias hidrográficas do nordeste do Pará ao noroeste do Maranhão a partir de imagens SRTM. In Proceedings of the 13th Simpósio Brasileiro de Sensoriamento Remoto, Florianópolis, Brazil, 21–26 April 2007; pp. 6827–6834.
48. Klein, E.L.; Moura, C.A.V. Síntese geológica e geocronológica do Cráton São Luís e do Cinturão Gurupi na região do rio Gurupi (NE-Pará/NW-Maranhão). *Geol. USP Ser. Cient.* **2003**, *3*, 97–112. [CrossRef]
49. Moraes, B.C.d.; Costa, J.M.N.D.; Costa, A.C.L.D.; Costa, M.H. Variação espacial e temporal da precipitação no Estado do Pará. *Acta Amaz.* **2005**, *35*, 207–214. [CrossRef]
50. Figueroa, S.N.; Nobre, C.A. Precipitations distribution over central and western tropical South América. *Climanálise* **1990**, *5*, 36–45.
51. Marengo, J.A. Interannual variability of deep convection over the tropical South American sector as deduced from ISCCP C2 data. *Int. J. Climatol.* **1995**, *15*, 995–1010. [CrossRef]
52. Pielke, R.A. *The Hurricane*; Routledge: New York, NY, USA, 1990.
53. Tölgyessy, J. The chemistry of water. In *Chemistry and Biology of Water, Air and Soil: Environmental Aspects*; Tölgyessy, J., Ed.; Elsevier Inc.: Amsterdam, The Netherlands, 1993; pp. 14–325.
54. American Public Health Association. *Standard Methods for the Examination of Water and Wastewater*, 19th ed.; American Public Health Association: Washington, DC, USA, 1995.
55. Luketina, D. Simple tidal prism models revisited. *Estuar. Coast. Shelf Sci.* **1998**, *46*, 77–84. [CrossRef]
56. Geyer, W.R.; Signell, R.; Kineke, G. Lateral trapping of sediment in a partially mixed estuaries. In *Physics of Estuaries and Coastal Seas, Proceedings of the 8th International Biennial Conference on Physics of Estuaries and Coastal Seas, 9–12 September 1996*; Dronkers, J., Scheffers, M., Eds.; A.A. Balkema: Rotterdam, The Netherlands, 1998; pp. 115–124.
57. Fernandes, L.L.; Rao, V.P.; Kessarkar, P.M.; Suresh, S. Estuarine turbidity maximum in six tropical minor rivers, central west coast of India. *Hydrol. Res.* **2018**, *49*, 1234–1254. [CrossRef]
58. Costa, M.S.; Rocha, A.S.; Santos, A.S.; Rollnic, M. Influence of tide on salt entrapment in the Mojuim River estuary. *J. Coast. Res.* **2018**, *85*, 81–85. [CrossRef]
59. Cooper, J.A. Geomorphology of Irish estuaries: Inherited and dynamic controls. *J. Coast. Res.* **2006**, *I*, 176–180.
60. Salomon, J.C.; Allen, G.P. Rôle sédimentologique de la marée dans les estuaires à fort marnage. *Cie. Fr. Petroles Notes Mem.* **1983**, *18*, 35–44.
61. Perillo, G.M.E.; Sequeira, M.E. Geomorphologic and sediment transport characteristics of the middle reach of the Bahia Blanca estuary (Argentina). *J. Geophys. Res.* **1989**, *94*, 14351–14362. [CrossRef]
62. Hayes, M.O. Morphology of sand accumulation in estuaries. In *Estuarine Research*; Cronin, L.E., Ed.; Academic Press: New York, NY, USA, 1975; pp. 3–22.
63. Souza-Filho, P.W.M. Avaliação e aplicação de dados de sensores remotos no estudo de ambientes costeiros tropicais úmidos, Bragança, norte do Brasil. Ph.D. Thesis, Universidade Federal do Pará, Belém, Brazil, 2000.
64. Hudson, A.S.; Talke, S.A.; Jay, D.A. Using satellite observations to characterize the response of estuarine turbidity maxima to external forcing. *Estuar. Coast.* **2017**, *40*, 343–358. [CrossRef]
65. Sommerfield, C.K.; Wong, K.C. Mechanisms of sediment flux and turbidity maintenance in the Delaware Estuary. *J. Geophys. Res. Ocean.* **2011**, *116*, 1–16. [CrossRef]
66. Dronkers, J.J. *Tidal Computations in Rivers and Coastal Waters*; North Holland Publishing: Amsterdam, The Netherlands, 1964.
67. North, E.W.; Houde, E.D. Retention of white perch and striped bass larvae: Biological-physical interactions in Chesapeake Bay estuarine turbidity maximum. *Estuaries* **2001**, *24*, 756–769. [CrossRef]
68. Kappenberg, J.; Grabemann, I. Variability of the mixing zones and estuarine turbidity maxima in the Elbe and Weser estuaries. *Estuaries* **2001**, *24*, 699–706. [CrossRef]